DFT modelling of oxygen adsorption on the Ag-doped $LaMnO_3$ (001) surface

A.U. Abuova[a], Yu. A. Mastrikov*[b], E. A. Kotomin[b], S. N. Piskunov[b], T.M. Inerbaev[a], A.T. Akylbekov[a]

[a]L.N. Gumilyov Eurasian National University, Mirzoyan str.2, Astana, Kazakhstan
[b]Institute of Solid State Physics, University of Latvia, Kengaraga str. 8, Riga, Latvia
*Corresponding author E-mail: yuri.mastrikov@cfi.lu.lv

By means of the DFT method, oxygen adsorption was calculated on the Ag-doped MnO_2- and LaO-terminated $LaMnO_3$ (001) surfaces. The catalytic effect of Ag-doping is shown by a comparison of adsorption energies, electron charge redistribution and interatomic distances for doped and undoped surfaces. Ag adsorption on MnO_2 terminated surface increases the adsorption energy for both atomic and molecular oxygen. This increases their surface concentrations and could improve the fuel cell cathode efficiency. The opposite effect takes place at the LaO terminated surface. Due to large adsorption energies, adsorbed oxygen atoms are immobile and the oxygen reduction reaction rate is controlled by concentration and mobility of oxygen vacancies

Keywords: solid oxide fuel cells, $LaMnO_3$, oxygen adsorption, Ag catalyst, *ab initio* calculations

1. Introduction

Rapidly growing demand for energy requires development of new sources of efficient, environmentally safe and sustainable sources of electric power. Solid Oxide Fuel Cells (SOFC) is a promising tool in this direction [1,2]. In SOFC hydrogen-based fuel is directly converted into electric power, producing water as a by-product. La*B*O_3 perovskites are well known as SOFC cathode material for their stability at high operation temperatures and compatibility with solid electrolyte. Oxygen adsorption on perovskite surfaces followed by dissociation and migration to anode (Oxygen Reduction Reaction, ORR) [3] is a limiting step on the SOFC cathode surfaces which occurs at quite high temperatures (> 800ºC). The ORR rate strongly depends on various factors, such as microstructure [4], defects [5] and doping [6,7].

In order to reduce the operation temperature down (e.g. 500ºC, Intermediate Temperature regime), use of catalysts is necessary [8]. The best catalyst for ORR is Pt or Pt-alloys, which, however, is quite expensive. Recent experimental studies [8,9] suggested Ag as an alternative. Zhou and co-authors [10,11] in their theoretical calculations have shown that on the MnO_2-terminated (001) $LaMnO_3$ (LMO) surface Ag-doping significantly increases oxygen adsorption energy. We also studied recently the effects of Ag adsorption at the LMO terminated surfaces for different catalyst concentrations [12].

So far, another (001) LMO termination - LaO surface- is much less studied. As it was shown [13], the ORR thereon strongly differ from that on the MnO_2 surface. Thus, in this paper, we performed first principles calculations of oxygen adsorption peculiarities on the Ag-doped LaO-terminated (001) LMO surface. In order to make a direct comparison of the adsorption parameters, we also revised the calculations on the MnO_2-terminated surface, and compared the results with those for undoped surfaces.

2. Computational Details

Modelling was performed by the computer code VASP 5.3.3 [14-16] with inner electrons described by Ultrasoft Potentials with the Projector Augmented Wave (PAW) method applied [17,18] (Table 1).

Table 1. VASP US PAW potentials used for La, Mn, O and Ag.

Potential	Plane wave basis set cut-off energy, eV	number of valence electrons	configuration
La	219.313	11	$5s^2 5p^6 6s^2 5d^1$
Mn_*pv*	269.864	13	$3p^6 4s^1 3d^6$
O	400.000	6	$2s^2 p^4$
Ag	249.844	11	$2s^1 d^{10}$

Perdew-Burke-Ernzerhof (PBE) [19] General Gradient Approximation (GGA) functional was used for exchange-correlation. Plane wave basis set cut-off energy was set to 520eV. Ferromagnetic order was chosen as the most stable one within the applied computational method. As it was shown in [20,21], the difference in adsorption energies does not depend on a particular magnetic state, except for diamagnetic one. The distortion of the perovskite structure is set as orthorhombic. The (001) $LaMnO_3$ surface was simulated as 7-plane LaO- or MnO_2-terminated slab. Dipole moment, normal to the surface, is naturally cancelled in such slabs. Surface supercell has extensions of $2\sqrt{2}a_0 \times 2\sqrt{2}a_0$, where a_0 is the lattice constant of pseudo-cubic perovskite. The process on the surface was symmetrically projected on both terminating planes, separated by the $5a_0$-large vacuum gap. The Brillouin zone was sampled by the 4×4×1 Monkhorst-Pack scheme [22]. Effective atomic charges were calculated by the Bader (topological) method [23].

3. Results and discussions

Adsorption of molecular oxygen was modelled on the Ag-doped (001) LMO surfaces. Ag-doping was simulated by placing single atom at the most energetically favourable sites [12]. The results are compared with those for undoped surface. Oxygen molecule was placed at the nearest to the dopant adsorption site. Adsorption energy was calculated with respect to oxygen in gaseous phase (the O_2 calculated binding energy is 5.9 eV). Adsorbed Ag atom is positively and negatively charged on the MnO_2 and LaO terminations, respectively, which considerably affects other ionic charges [12].

3.1.Oxygen adsorption on the Ag-doped (001) MnO_2-terminated LMO surface

3.1.1.Molecular adsorption

The most favourable adsorption site on this termination for molecular oxygen is atop of Mn atom. Tilted orientation is more stable than that parallel to the surface [20]. Oxygen molecule on the Ag-doped surface appears to be more stable by 0.26 eV (**Table 2**). Doping promotes higher charge transfer for more distant to the surface oxygen atom (-0.14 *e*) via surface Mn atom (+0.14 *e*). Molecular bond becomes 2% longer. In both cases molecule is in the charge state of superoxide O_2^-.

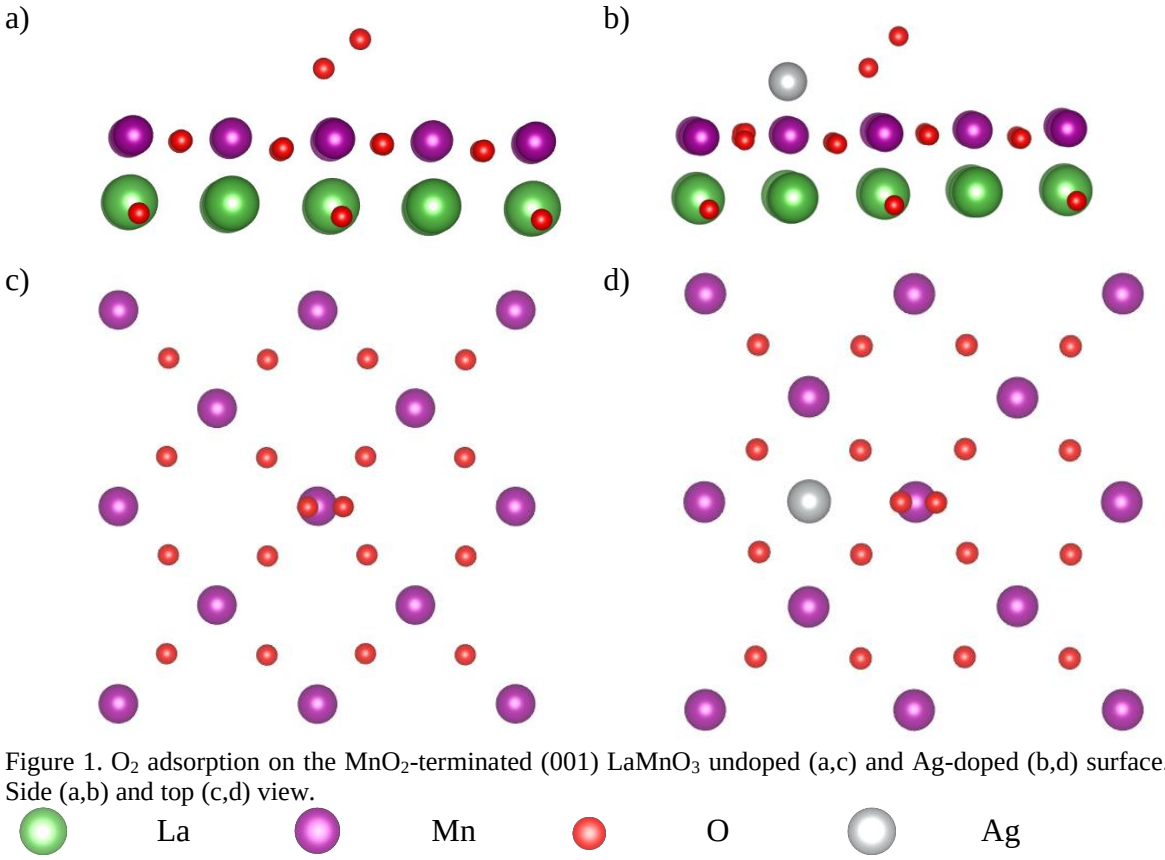

Figure 1. O_2 adsorption on the MnO_2-terminated (001) $LaMnO_3$ undoped (a,c) and Ag-doped (b,d) surface. Side (a,b) and top (c,d) view.

Table 2. O_2 adsorption on the MnO_2-terminated (001) $LaMnO_3$ undoped and Ag-doped surface. $O_{(1)}$ – closer- , $O_{(2)}$ – more distant to the surface atoms of adsorbed O_2 molecule.

Surface	E_{ads}, eV	Distance, Å		Bader charge, *e*			Mn averaged charge, *e*		Ag charge, *e*	
		$O_{(1)}$-$O_{(2)}$	$O_{(1)}$-Mn	$O_{(1)}$	$O_{(2)}$	Mn	prior O_2 ads.	after O_2 ads.	prior O_2 ads.	after O_2 ads.
undoped (Figure 1a,c)	-1.47 (O_2 binding energy 5.9 eV) -0.298 [10] -1.13 [21]	1.28 1.28 [10] 1.36 [21]	1.89 2.06[10] 1.86 [21]	-0.24 0.16 [10] -0.29 [21]	-0.12 -0.11 [10] -0.13 [21]	1.65 0.93 [10] 1.78 [21]	1.73	1.74		
Ag doped (Figure 1b,d)	-1.73 -1.11 [10]	1.30 1.33 [10]	1.92 2.02 [10]	-0.38 -0.21 [10]	-0.13 -0.21 [10]	1.79 0.89 [10]	1.71	1.72	0.57	0.63 0.38 [10]

Doping effect could be illustrated by means of difference electron density maps, plotted with respect to isolated adsorbate and undoped, as well as Ag-doped adsorbent. Thus, the interaction between the dopant and the surface is eliminated from the plots. The maps show the charge transfer between the ions in the terminating plane on undoped and doped surfaces.

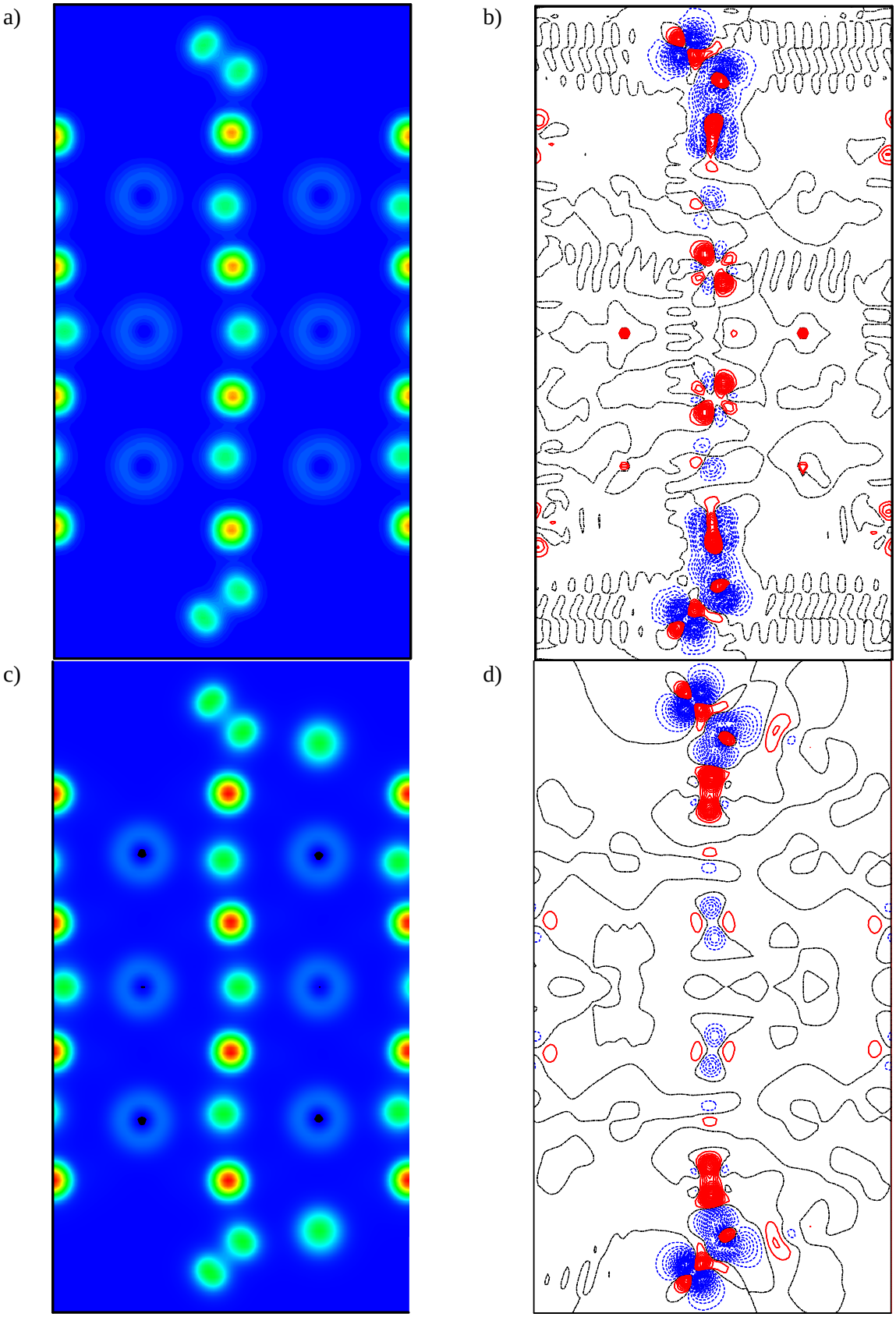

Figure 2.Total (a) (c) and difference (b) (d) electron density maps of O_2 on undoped (a) (b) and Ag-doped (c) (d) MnO_2-terminated (001) LMO surface.

Oxygen molecule receives the main portion of electron charge (dashed (blue in colour) isolines) from the surface Mn ion (solid (red in colour version) isolines). Ag atom supplies the surface Mn ions with additional electron charge. Also it provides a small amount of charge for adsorbed O_2 (solid (red in colour version) isolines) (Figure 2b,d).

3.1.2. *Atomic adsorption*

Atomic adsorption was modelled in two (for undoped) and three (for doped surface configurations). Single O atom was placed atop surface Mn atom (Figure 3a,c), at the closest distance from Ag atom for doped surface (Figure 3b,d). Two O atoms were placed atop two neighbouring Mn atoms (Figure 3e,g). The distance to Ag atom for two O atoms was varied from the closest equal (Figure 3f,h) to a combination of the closest and the distant (Figure 3i,j).

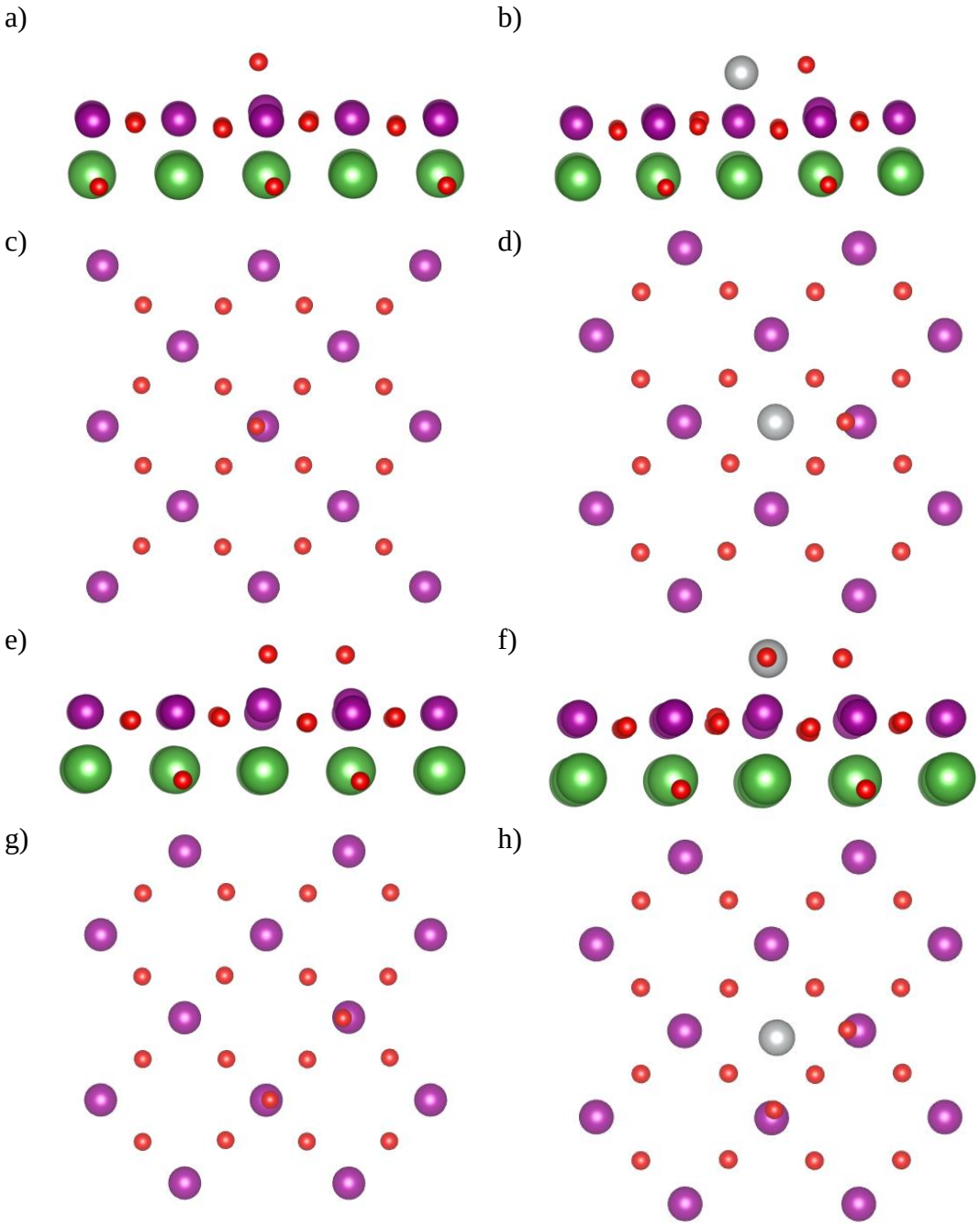

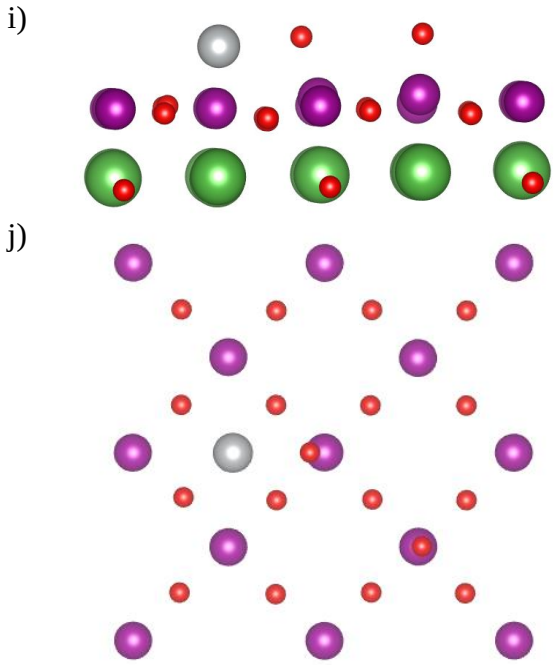

Figure 3**.** Atomic oxygen adsorption on the undoped (a,c,e,g) and Ag doped (b,d,f,h,i,j) (001) MnO_2 surface, side (a,b,e,f,i) and top (c,d,g,h,j) view.

Table 3. Atomic adsorption of single O atom on the MnO_2-terminated (100) LMO surface.

Surface, configuration	E_{ads}, eV	Distance, Å	Bader charge, *e*	
		O-Mn	O	Mn
undoped, single O (Figure 3a,c)	-1.18 -1.75[24] -1.07 [21]	1.61 1.60 [24] 1.63 [21]	-0.62 -0.63 [21]	1.85

Table 4. Atomic adsorption of single O atom on Ag-doped MnO_2-terminated (100) LMO surface.

Surface, configuration	E_{ads}, *e*V	Distance, Å		Bader charge, *e*		
		O-Ag	O-Mn	O	Mn	Ag
doped, single O (Figure 3b,d)	-2.02 -0.934*[11]	2.22 2.19[11]	1.69 1.75[11]	-0.82 -1. 49 [11]	1.81 0.82 [11]	0.62 042 [11]

* adsorption on the LSM surface

Table 5. Atomic adsorption of two O atoms ($O_{(1)}$ and $O_{(2)}$) atop two surface Mn atoms ($Mn_{(1)}$ and $Mn_{(2)}$) on the MnO_2-terminated (100) LMO surface.

Surface, configuration	E_{ads}, *e*V	Distance, Å			Bader charge, *e*			
		$O_{(1)}$-$O_{(2)}$	$O_{(1)}$-$Mn_{(1)}$	$O_{(2)}$-$Mn_{(2)}$	$O_{(1)}$	$O_{(2)}$	$Mn_{(1)}$	$Mn_{(2)}$
undoped, two O atoms atop 1NN Mn (Figure 3e,g)	-2.32	3.62	1.60	1.60	-0.55	-0.55	1.82	1.82

Table 6. Atomic adsorption of two O atoms ($O_{(1)}$ and $O_{(2)}$) atop two surface Mn atoms ($Mn_{(1)}$ and $Mn_{(2)}$) on Ag-doped MnO_2-terminated (100) LMO surface.

Ads. Site	E_{ads}, *e*V	Distance, Å					Bader charge, *e*				
		$O_{(1)}$-Ag	$O_{(2)}$-Ag	$O_{(1)}$-$O_{(2)}$	$O_{(1)}$-$Mn_{(1)}$	$O_{(2)}$-$Mn_{(2)}$	$O_{(1)}$	$O_{(2)}$	$Mn_{(1)}$	$Mn_{(2)}$	Ag

doped, two O atoms at the same distant from Ag atom (Figure 3f,h)	-3.49	2.23	2.27	3.41	1.66	1.66	-0.75	-0.73	1.83	1.83	0.70
doped, two O atoms at different distances from Ag atom (Figure 3i,j)	-3.17	2.23	6.08	4.22	1.68	1.60	-0.80	-0.56	1.81	1.80	0.63

Atomic adsorption energies suggest dissociative O_2 adsorption on the MnO_2 termination with the energy gain of 0.89 eV for undoped and 1.47 eV for doped surface. Ag doping increases adsorption energy of a single atom by 0.84 eV. Interaction between O atoms on undoped surface is practically negligible. On the doped surface, two O atoms placed close to the dopant, demonstrate repulsion interaction of 0.27 eV per atom. No interaction was observed between two oxygen atoms at the same relative distance, with one O placed closer to Ag atom. For a single oxygen, as well as two oxygen atoms at the same distance from Ag, the charge transfer to O is higher by 0.2 *e* on the doped surface.

3.2. Oxygen adsorption on the Ag-doped (001) LaO-terminated LMO surface

3.2.1. Molecular adsorption

On LaO termination molecule is stable at hollow position in two orientations – tilted and parallel to the surface. The most energetically favourable of two "hollow" positions for atomic adsorption has been chosen for modelling of molecular adsorption. In tilted orientation oxygen molecule forms one short and one long bond to the nearest two surface La atoms (Figure 4).

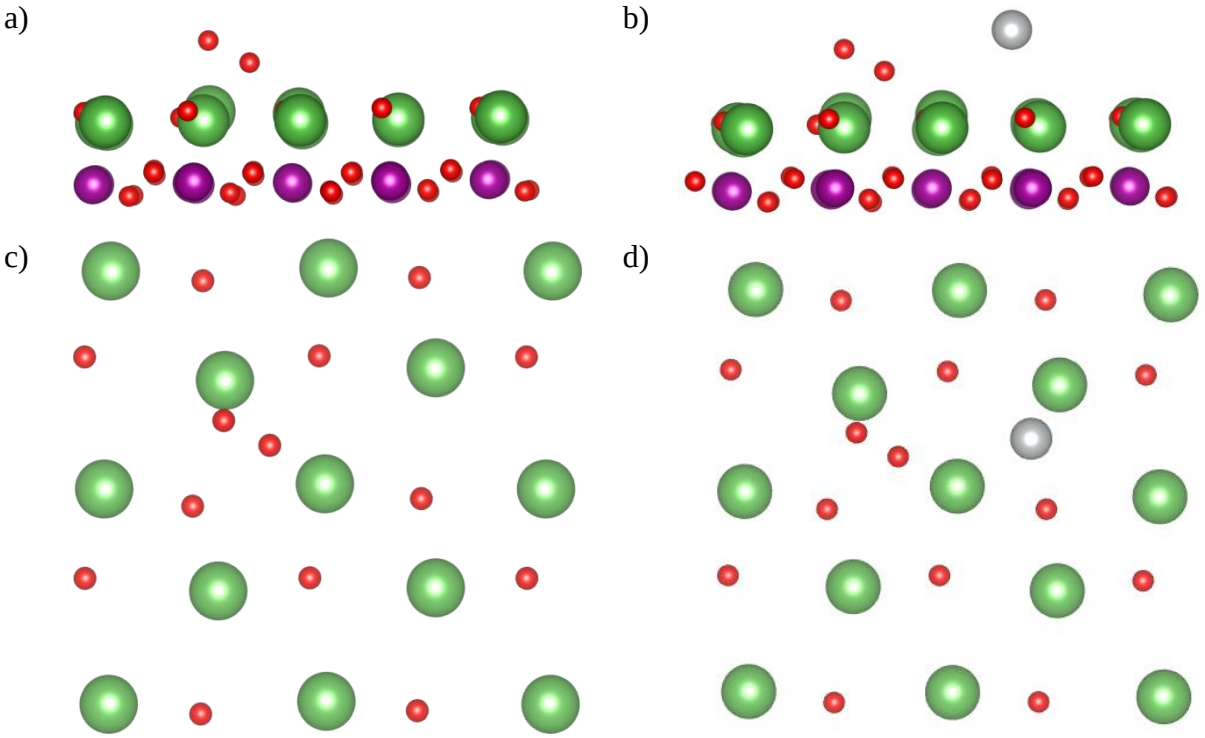

Figure 4. O_2 molecule adsorption in tilted orientation on the LaO-terminated (001) $LaMnO_3$ undoped (a,c) and Ag-doped (b,d) surface.Side (a,b) and top (c,d) view.

Ag doping decreases the adsorption energy by 0.46 eV (Table 7). For more favourable adsorbed molecule orientation, parallel to the surface (Figure 7), doping decreases adsorption energy too by 0.31 eV (Table 8).

Like for the tilted orientation on the LaO termination, charge transfer and bond length changes due to the doping are negligibly small (Figure 5 and Figure 6).

In a comparison to the MnO_2 termination, charge transfer between the adsorbent and adsorbate on the LaO termination is higher. Interacting predominantly by one atom, oxygen molecule in the tilted configuration is in the state of superoxide O_2^-, whereas in parallel configuration both atoms form bonds with the surface La atoms, making adsorbent peroxide O_2^{2-}.

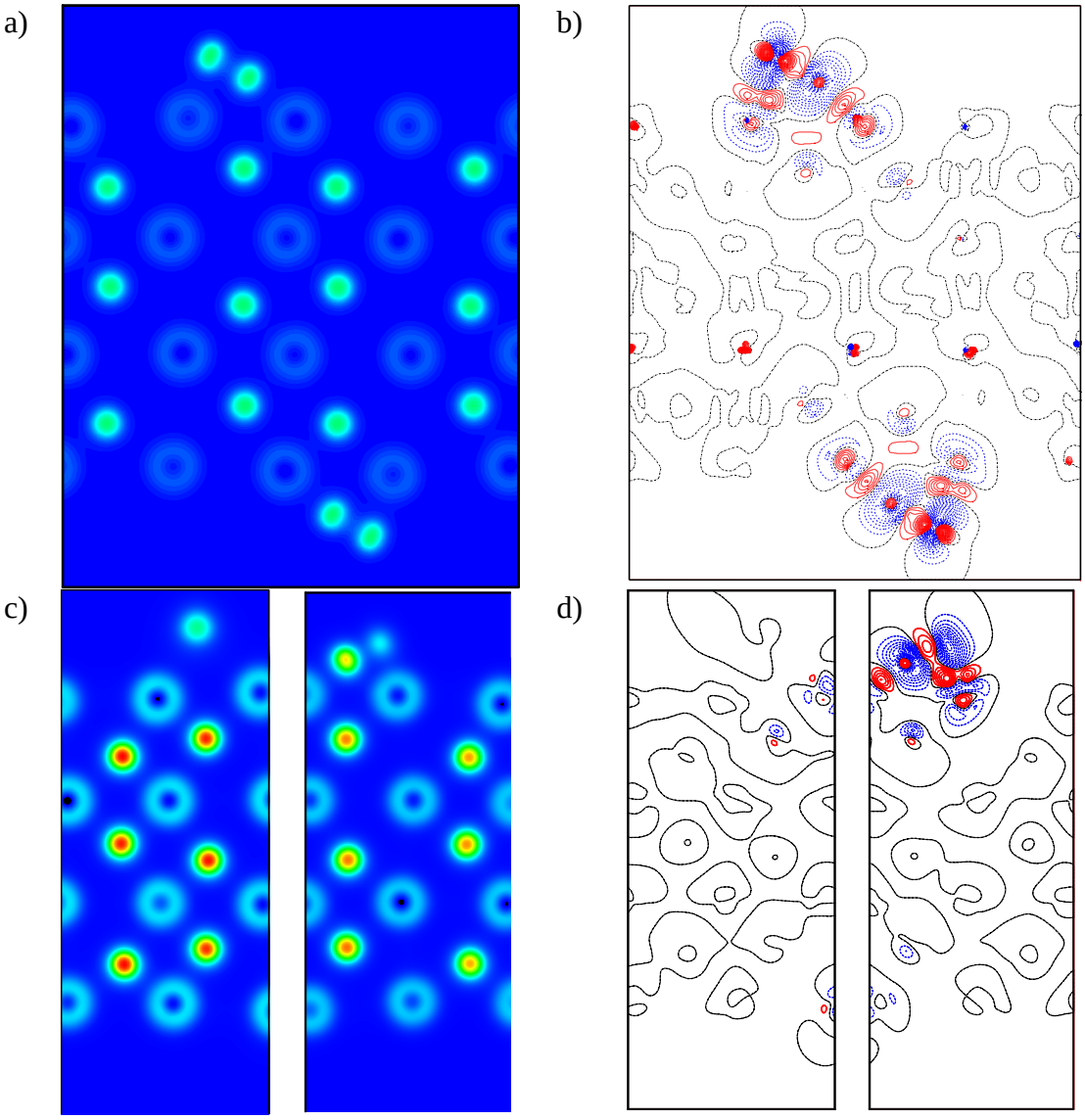

Figure 5. Total (a) (c) and difference (b) (d) electron density maps of tilted O_2 on undoped (a) (b) and Ag-doped (c) (d) LaO-terminated (001) LMO surface.(Ag atom on the left-hand side).

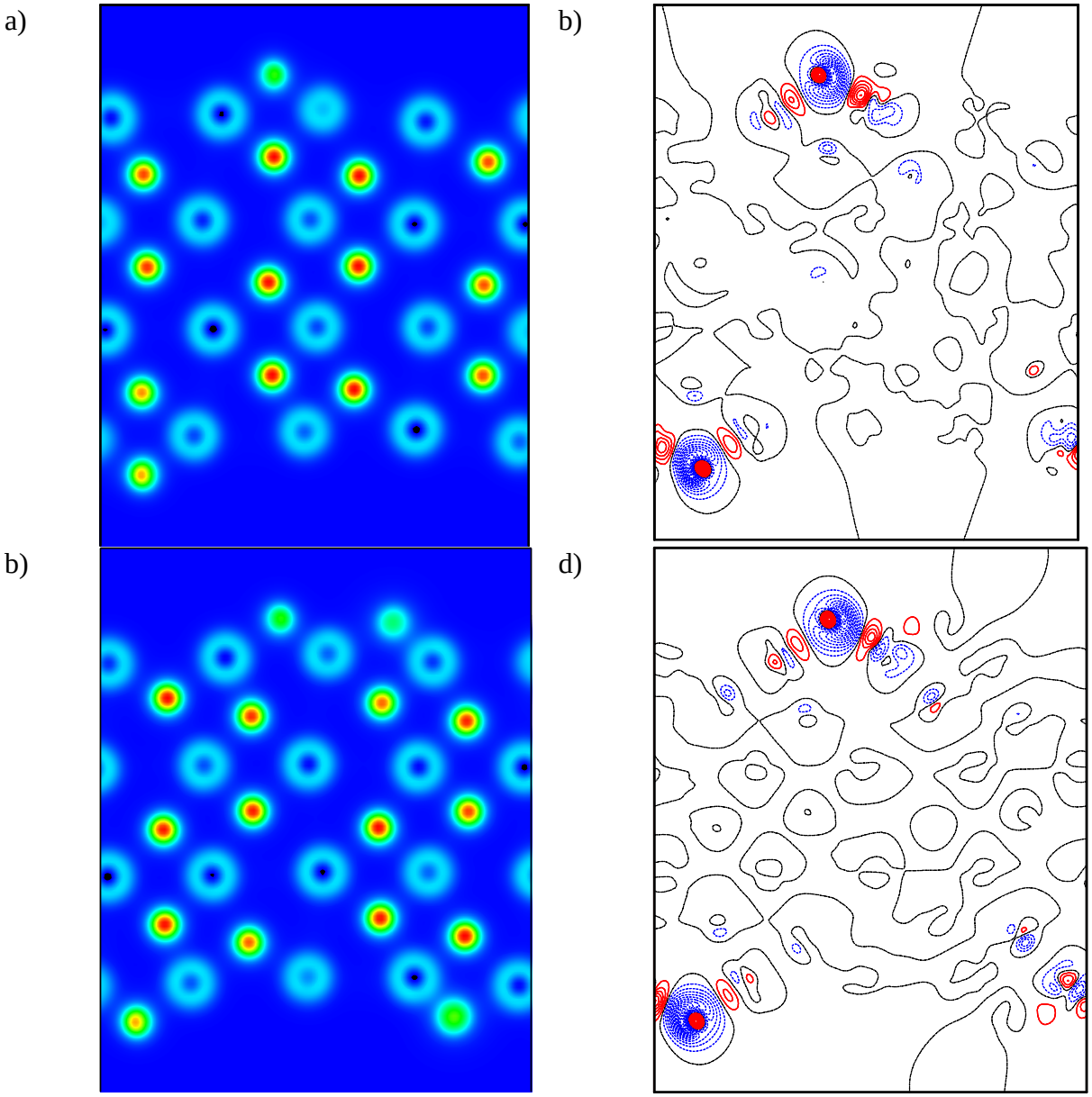

Figure 6. Total (a) (c) and difference (b) (d) electron density maps of parallel to the surface O_2 on undoped (a) (b) and Ag-doped (c) (d) LaO-terminated (001) LMO surface.(Ag atom on the rigt-hand side).

Table 7. O_2 adsorption in tilted orientation on the LaO-terminated (001) $LaMnO_3$ undoped and Ag-doped surface. $O_{(1)}$ – closer - and $O_{(2)}$ – more distant to the surface $La_{(1)}$ atoms of O_2. $La_{(2)}$ is the nearest to $O_{(2)}$ atom.

Ads. site	E_{ads}, *e*V	Distance, Å				Bader charge, *e*				Mn averaged charge, *e*		Ag charge, *e*	
		$O_{(1)}$-$O_{(2)}$	$O_{(1)}$-$La_{(1)}$	$O_{(2)}$-$La_{(1)}$	$O_{(2)}$-$La_{(2)}$	$O_{(1)}$	$O_{(2)}$	$La_{(1)}$	$La_{(2)}$	prior O_2 ads.	after O_2 ads.	prior O_2 ads.	after O_2 ads.
undoped (Figure 4a,c)	-4.50 -0.71[11] -3.20[25]	1.48 1.30[11] 1.36[25]	2.27	2.45	2.25 2.60[11]	-0.62 -0.14[11]	-0.73 -0.28[11]	2.03 2.29[25]	2.03	1.60	1.63		
Ag-doped (Figure 4b,d)	-4.03	1.46	2.25	2.42	2.23	-0.60	-0.71	2.03	2.02	1.62	1.65	-0.69	-0.64

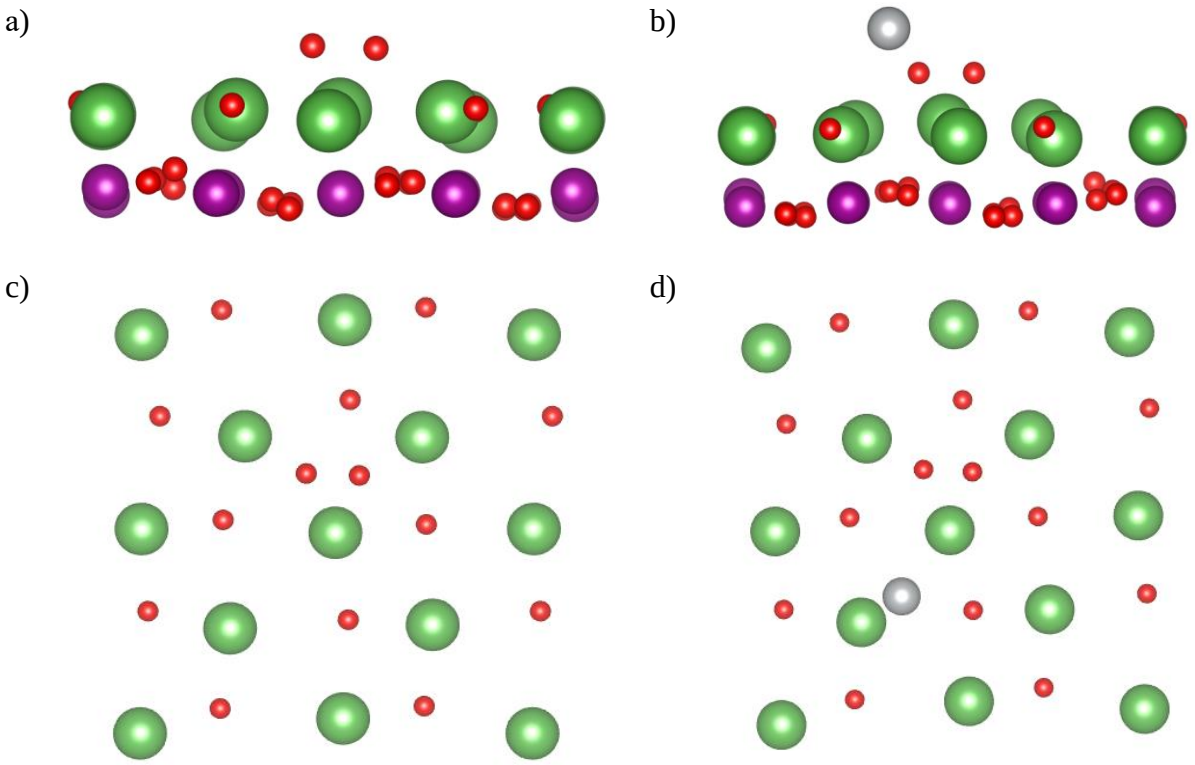

Figure 7. O_2 molecule adsorption in parallel to the surface orientation on the LaO-terminated (001) $LaMnO_3$ undoped (a) and Ag-doped (b) surface. Side (a,b) and top (c,d) view.

Table 8. O_2 adsorption in parallel to the surface orientation on the LaO-terminated (001) $LaMnO_3$ undoped and Ag-doped surface. $La_{(1)}$ is close to both $O_{(1)}$ and $O_{(2)}$ atoms, $La_{(2)}$ and $La_{(3)}$ are close and distant to $O_{(1)}$ and $O_{(2)}$ atoms, respectively.

Ads. site	E_{ads}, *e*V	Distance, Å					Bader charge, *e*					Mn averaged Charge, *e*		Ag charge, *e*	
		$O_{(1)}$-$O_{(2)}$	$O_{(1)}$-$La_{(1)}$	$O_{(1)}$-$La_{(2)}$	$O_{(2)}$-$La_{(1)}$	$O_{(2)}$-$La_{(3)}$	$O_{(1)}$	$O_{(2)}$	$La_{(1)}$	$La_{(2)}$	$La_{(3)}$	prior O_2 ads.	after O_2 ads.	prior O_2 ads.	after O_2 ads.
undoped (Figure 7a,c)	-4.50	1.48	2.31	2.57	2.38	2.48	-0.73	-0.66	2.02	2.01	2.06	1.59	1.63		
Ag doped (Figure 7b,d)	-4.21	1.48	2.31	2.49	2.39	2.44	-0.69	-0.67	2.01	2.03	2.06	1.61	1.65	-0.69	-0.66

3.2.2. Atomic adsorption

Atomic adsorption was modelled for one and two O atoms close to Ag atom. Two oxygen atoms were places at the first annd second nearest adsorption sites. For all configurations on the LaO termination, Ag doping reduces the adsorption energy. Oxygen atoms repel each other on both undoped and doped surfaces. The electron charge on adsorbed O atoms varies in a range of -1.2e to -1.27 *e*. Charge exchange with Ag atom is also small (-0.62*e*...-0.69 *e*).

Table 9. Adsorption of single O atom between two - $La_{(1)}$ and $La_{(2)}$ atoms on undoped and Ag-doped LaO-terminated (100) LMO surface.

Surface, configuration	E_{ads}, *e*V	Distance, Å		Bader charge, *e*			
		O-$La_{(1)}$	O-$La_{(2)}$	O	$La_{(1)}$	$La_{(2)}$	Ag
undoped, single O atom (Figure 8a,c)	-3.98 -4.57[24] -2.51[25]	2.19 2.15[24] 2.23[25]	2.17	-1.25 -1.35[25]	2.01 2.28[24]	2.01	
doped, single O atom (Figure 8b,d)	-3.57	2.16	2.15	-1.22	2.01	2.02	-0.66

Table 10. Adsorption of two $O_{(1)}$ and $O_{(2)}$ atoms on undoped LaO-terminated (100) LMO surface. $La_{(1)}$ is located between two adsorbed O atoms.

Surface, configuration	E_{ads}, *e*V	Distance, Å			Bader charge, *e*		
		$O_{(1)}$-$O_{(2)}$	$O_{(1)}$- $La_{(1)}$	$O_{(2)}$-$La_{(1)}$	$O_{(1)}$	$O_{(2)}$	$La_{(1)}$
undoped, two O atoms 1NN (Figure 8e,g)	-6.70	3.28	2.14	2.18	-1.22	-1.23	1.99
undoped, two O atoms 2NN (Figure 8i,k)	-7.41	4.06	2.24	2.26	-1.27	-1.26	2.03

Table 11. Adsorption of two $O_{(1)}$ and $O_{(2)}$ atoms on the Ag-doped LaO-terminated (100) LMO surface. $La_{(1)}$ is located between two adsorbed O atoms.

Surface, configuration	E_{ads}, *e*V	Distance, Å			Bader charge, *e*			
		$O_{(1)}$-$O_{(2)}$	$O_{(1)}$-$La_{(1)}$	$O_{(2)}$-$La_{(1)}$	$O_{(1)}$	$O_{(2)}$	$La_{(3)}$	Ag
doped, two O atoms 1NN (Figure 8f,h)	-6.39	3.38	2.13	2.21	-1.23	-1.23	1.98	-0.65
doped, two O atoms 2NN (Figure 8j,l)	-6.58	4.15	2.24	2.23	-1.24	-1.24	2.03	-0.62

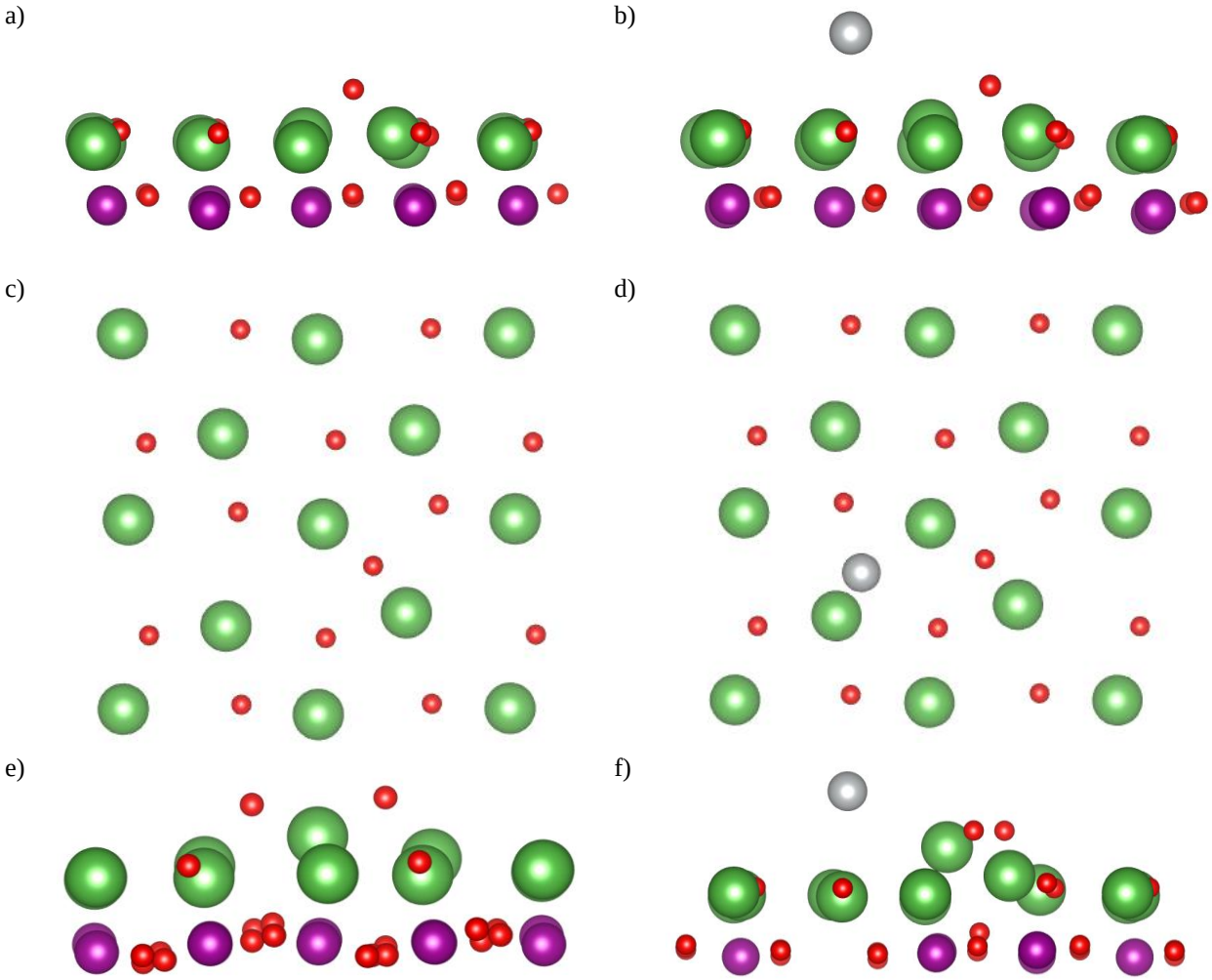

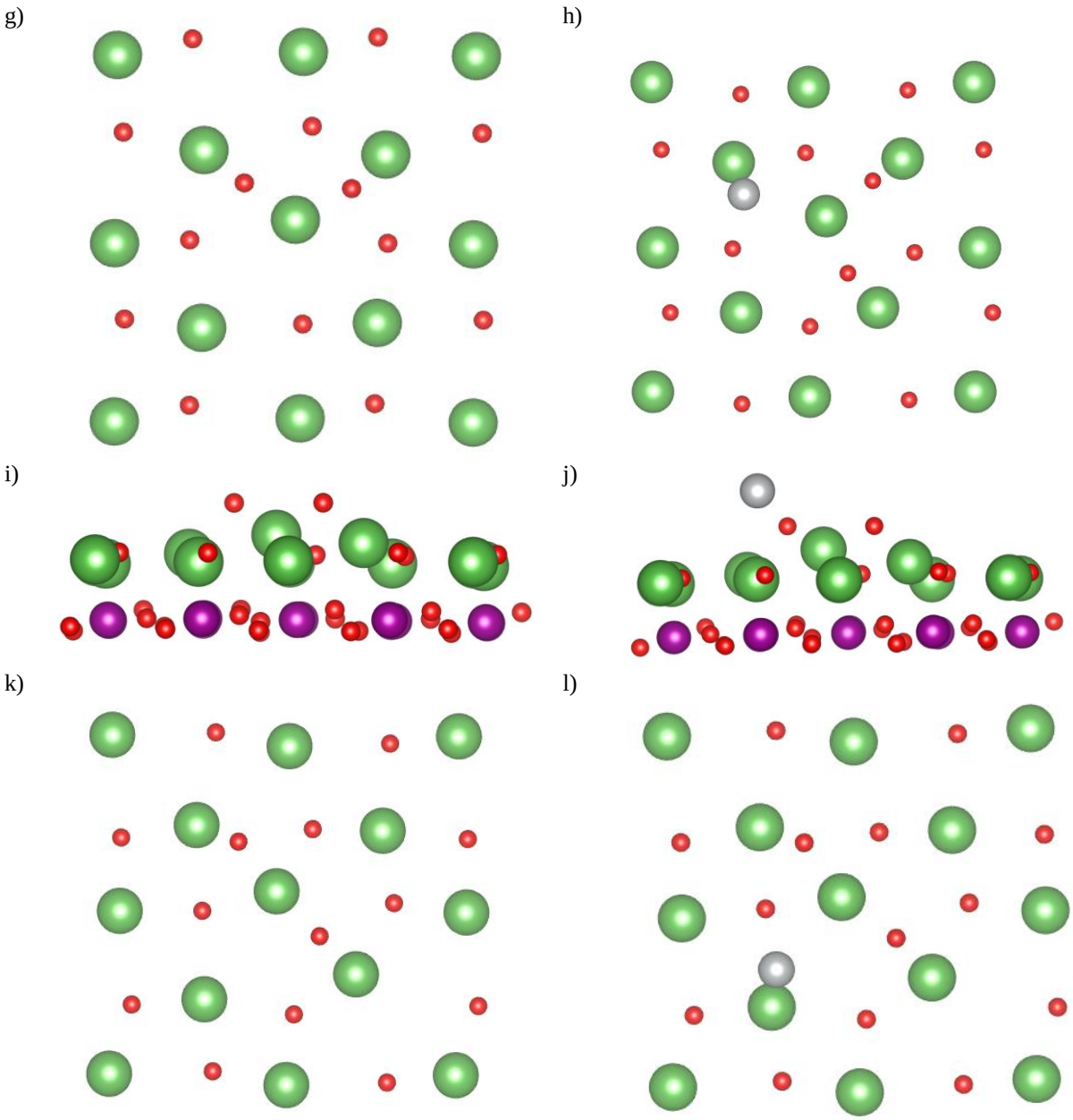

Figure 8. Atomic adsorption of one (a-d) and two (e-l) oxygen atoms on undoped (a,c,e,g,i,k) and Ag-doped (b,d,f,h,j,l) LaO-terminated surface. Side (a,b,e,f,i,j) and top (c,d,g,h,k,l) view.

In tilted configuration on the LaO-terminated surface, oxygen molecule receives electron charge (dashed (blue in colour) isolines) from two surface La ions (solid (red in colour version) isolines). For the Ag-doped slab surface, La ions become more positive, providing less electron charge (dashed (blue in colour) isolines) for adsorbed O_2 molecule.

Conclusions

We have shown in this paper, that the two possible terminations of the $LaMnO_3$ (001) surface reveal quite different properties (which is in line with our previous studies [13, 25, 27]. Doping with Ag makes both, MnO_2- as well as LaO-terminated, surfaces less polar. For MnO_2 termination with overcharged cations Ag provides additional charge, which makes Mn cations less positive. Less positive Mn cations donate that additional charge to adatom, facilitating adsorption. For LaO termination Ag doping does the opposite – undercharged La

cations become more positive, which makes adsorption of oxygen less energetically efficient. Low adsorpion energies on the MO_2 termination increase and high adsorption energies on the LaO termination decrease. As a doping material on LMO surface, Ag exhibited a unique ability to change the polarity of the own charge, making nonstoichiometric slabs more stable. Ag doping makes, initially less favourable for oxygen adsorption, MnO_2-terminated LMO surface more catalytically active.

With respect to the oxygen reduction reaction on fuel cell cathode, Ag adsorption on MnO_2 terminated surface increases the adsorption energy for both atomic and molecular oxygen, increases their surface concentration [13,28] and thus improves the cathode efficiency. Due to very large adsorption energies, adsorbed oxygen atoms are immobile and the ORR is controlled by concentration and mobility of oxygen vacancies [1,21]. In turn, on the LaO termination Ag doping decreases the adsorption energies and oxygen concentrations. This hardly play an essential role in the ORR here, since surface oxygen concentration on this surface even without doping is five orders of magnitude smaller than on the MnO_2 terminated surface [21] and thus this termination does not contribute to the ORR. Ag doping plays here a negative role.

Acknowledgements

This study was partly financed by the State Education Development Agency of the Republic of Latvia via the Latvian State scholarship (AA) and Latvia-Ukraine project (grant LV-UA/2018/2 to EK). Authors thank M. Sokolov for technical assistance and valuable suggestions.

References

1. M.M. Kuklja, E.A. Kotomin, R. Merkle, Yu. Mastrikov, J. Maier, Phys. Chem. Chem. Phys. **15**, 5443 (2013).
2. E.A. Kotomin, R. Merkle, Yu. Mastrikov, M.M. Kulkja, J. Maier, chapter 6 in a book *Computational Approaches to Energy Materials* (ed. A. Walsh, A.A. Sokol, C.R.A. Catlow), John Wiley, 2013.
3. E. Ahmad, V. Tileli, D. Kramer, et al, J. Phys. Chem. C **119**, 16804 (2015).
4. A.S. Farlenkov, M.V. Ananyev, V.A. Eremin, N.M. Porotnikova, E.Kh. Kurumchin, Fuel Cells, 15(1), pp. 131-139, (2015).
5. N.M. Porotnikova, M.V. Ananev, E.Kh. Kurumchin, Russian Journal of Electrochemistry, 47(11), pp. 1250-1256, (2011).
6. N.M. Porotnikova N.M., M.V. Ananyev, V.A. Eremin, N.G. Molchanova, E.Kh. Kurumchin, Effect of acceptor substitution in perovskites $La_{1-x}A_xMnO_{3\pm\delta}$ (A = Ca, Sr, Ba) on the kinetics of interaction of gas-phase oxygen. Russian Journal of Electrochemistry 52(8), pp. 717-722, (2016).
7. N.M. Porotnikova, V.A. Eremin, A.S. Farlenkov, E.Kh. Kurumchin, E.A. Sherstobitova, D.I. Kochubey, M.V. Ananyev., Effect of AO segregation on catalytical activity of $La_{0.7}A_{0.3}MnO_{3\pm\delta}$ (A = Ca, Sr, Ba) regarding oxygen reduction reaction. Catalysis Letters, 148(9), pp. 2839-2847, (2018).
8. H.J. Choi, M. Kim, K. Ch. Neoh, et al, Adv. Energy Mater., **7**, 1601956 (2017).
9. S.-A. Park, E.-K. Lee, H. Song, Y.-T. Kim, Scientific Reports, **5**, 13552 (2015).
10. Y. Zhou, Z. Lü, P. Guo, Y. Tian, X. Huang, W. Su, Appl. Surf. Sci. **258**, 2602 (2012).

11. Y. Zhou, Z. Lü, B. Wei, X. Zhu, X. Huang, W. Jiang, and W. Su, J. Power Sources 209, 158 (2012).
12. A.U. Abuova, Yu. Mastrikov, E.A. Kotomin, Y. Kawazoe, T.M. Inerbaev, A.T. Akilbekov, Solid State Ionics 273, 46 (2015).
13. Yu. Mastrikov, R. Merkle, E.A. Kotomin, M.M. Kuklja, J. Maier, J. Mater. Chem. A 6, 11929 (2018).
14. G. Kresse and J. Furthmueller, Phys. Rev. B **54**, 11169 (1996).
15. G. Kresse and J. Furthmüller, Comp. Mater. Sci. **6**, 15 (1996).
16. G. Kresse and J. Hafner, Phys. Rev. B **47**, 558 (1993).
17. P.E. Blöchl, Phys. Rev. B **50**, 17953 (1994).
18. G. Kresse, and J. Joubert, Phys. Rev. B **59**, 1758 (1999).
19. J.P. Perdew, K.Burke, and M.Ernzerhof, Phys. Rev. Lett. **77**, 3865 (1996).
20. Yu. A. Mastrikov, PhD thesis, University of Stuttgart, Germany (2008).
21. E. A. Kotomin, Yu. Mastrikov, E. Heifets, J. Maier, Phys. Chem. Chem. Phys. 10, 4644 (2008).
22. H. J. Monkhorst and J. D. Pack, Phys. Rev. B **13**, 5188 (1976).
23. M. Yu and D. R. Trinkle, J. Chem. Phys. **134**, 064111 (2011).
24. G.Pilania, R.Ramprasad, Surface Science **604**, 1889 (2010).
25. S. Piskunov, T.Jacob, E. Spohr, Physical Review B 83, 073402 (2011)
26. R.A. Evarestov, E.A. Kotomin, Yu. Mastrikov, D. Gryaznov, E. Heifets, J. Maier. Phys. Rev. B **72**, 214411 (2005)
27. S. Piskunov, E. Heifets, T. Jacob, E.A. Kotomin, D. Ellis, E. Spohr. Phys. Rev. B **78**, 121406 (2008)
28. Yu. Mastrikov, R. Merkle, E. Heifets, E.A. Kotomin, J. Maier. J. Phys. Chem. C **114**, 3017 (2010).

Institute of Solid State Physics, University of Latvia as the Center of Excellence has received funding from the European Union's Horizon 2020 Framework Programme H2020-WIDESPREAD-01-2016-2017-TeamingPhase2 under grant agreement No. 739508, project CAMART²